

ELECTRONIC SUPPLEMENTARY INFORMATION (ESI)

NFC-Enabled Photothermal-Based Microfluidic Paper Analytical Device for Glucose Detection

Kawin Khachornsakkul,^{1,2*} Ruben Del-Rio-Ruiz,^{1,2} Cihan Asci,^{1,2} Sameer Sonkusale^{1,2*}

¹ *Department of Electrical and Computer Engineering, Tufts University, Medford, MA 02155,
USA*

² *Nano Lab, Tufts University, Medford, MA 02155, USA*

**To whom correspondence should be addressed. Email: Kawin.khachornsakkul@tufts.edu
sameer.sonkusale@tufts.edu*

Table of Contents

Preparation solutions	S3
Design and fabrication of the portable NFC platform	S4
Fig. S1 AuNP characteristics.	S7
Fig. S2 Absorption spectrum and TEM image of AuNPs with PBS and glucose solution.	S8
Fig. S3 Photothermal analysis on μ PADs for blank and glucose detection.	S9
Fig. S4 Reaction time studies.	S10
Fig. S5 Irradiation time studies.	S11
Fig. S6 Investigation of the paper spot format	S12
Fig. S7 Reproducibility measurement.	S13
Fig. S8 The linear range of glucose detection with colorimetric method	S14
Fig. S9 Selectivity and interferent effect	S15
Fig. S10 Storage time.	S16
Table S1 Recovery studies in human control serum and artificial saliva samples	S17
Fig. S11 Sample matrices studies	S18

Preparation of solution

Phosphate buffer (50.0 mmol L⁻¹, pH 7.4) was prepared by mixing Na₂HPO₄ and NaH₂PO₄ with deionized (DI) water, and then adjusting the pH with NaOH (0.20 mol L⁻¹) and/or HCl (0.20 mol L⁻¹).

Artificial saliva samples were prepared by mixing KH₂PO₄ (2.50 mmol L⁻¹), Na₂HPO₄ (2.40 mmol L⁻¹), KHCO₃ (15.0 mmol L⁻¹), NaCl (10.0 mmol L⁻¹), MgCl₂ (1.50 mmol L⁻¹), CaCl₂ (1.50 mmol L⁻¹) and citric acid (0.15 mmol L⁻¹) and adjusted to pH 6.7 with NaOH (0.20 mol L⁻¹) and/or HCl (0.20 mol L⁻¹).³³

Design and fabrication of the portable NFC platform

The integration of the μ PADs with NFC technology is accomplished using SolidWorks (Dassault Systems SolidWorks Corporation, Waltham, MA), as illustrated in **Fig. 1**. The device comprises a 3D-printed platform designed to create a portable, NFC-enabled, smartphone-based photothermal analytical sensing device. This platform is strategically engineered to facilitate the integration of all components in a rapid, cost-effective, and compact form factor.

The circuit schematic for the platform is outlined as follows (**Fig. 1a**): A customized battery charging system enables the selection of current flow between two different states. The first state (active mode) allows current flow between a 3.7V 2Ah LiPo rechargeable battery (LP103454) and a high-power LED that emits light at a wavelength of 535nm, boasting a maximum luminous flux of 260lm. Additionally, a pre-wired 2-pin position snap switch (B09TDHJDBQ) is utilized to control LED activation. A current limiter resistor is also incorporated in series between the snap switch and the LED, preventing the battery source from exceeding the LED's 1.5A current limit. The second state (charging mode) allows current flow between a USB connector and the battery to charge the battery. Consequently, this customized charging circuit facilitates a seamless control between LED power and battery charging states, enhancing the overall portability of the platform, and eliminating the need to replace or externally recharge the drained LiPo battery. Furthermore, the battery charger circuit incorporates readily available components, including a lithium-ion battery protection circuit to safeguard against overcharging or overcurrent. The charge current is programmable and capped at a maximum of 900 mA with an external resistor, although this maximum current may be constrained by the USB source. Additionally, a Double Pole Double Throw (DPDT) mechanical switch is included to enable the flow of current between battery charging and LED powering

modes, as shown in **Fig. 1a**. In the active mode, when the mechanical DPDT switch is engaged, and the snap switch is shorted, the LED emits light in the 535nm wavelength visible spectrum directly onto the detection zone of the μ PADs. This process elevates the temperature of the paper, and the degree of temperature rise is indicative of the sample concentration. Sequentially, the temperature sensor embedded in the commercially available SmarTag1 NFC board is strategically placed behind the detection zone of the μ PADs (**Fig. 1b, c, and d**). This positioning enables efficient sensing of the temperature increase resulting from the reaction of the μ PADs. The SmarTag1 NFC system is configured to operate in a battery-less mode, aiming to minimize the overall system's battery consumption. This is achieved by employing the ST25DV64K dynamic NFC tag solution. When an NFC-enabled smartphone is brought close to the platform, it electromagnetically powers the SmarTag1 system, reads the temperature of the sensor, and promptly transmits the temperature value to the application installed on the smartphone. This concept facilitates a simple and rapid process for sensing the concentration of the introduced solution. Importantly, it eliminates the need for a battery, making the sensing system independent of external energy sources.

The platform is thoughtfully designed to streamline both its assembly and functionality efficiently. In a bottom-to-top arrangement within the platform (**Fig. 1b**), the battery occupies the first slot, followed by the battery charger circuitry system. The SmartTag1 NFC system is inserted into the second slot of the platform. The LED measuring 1x1 mm is affixed to the tip of a flexible structure (**Fig. 1b, c**) to maintain a fixate distance between the LED, the detection zone of the paper sensor, and the temperature sensor imbedded in the SmarTag1 (**Fig. 1c, d**). Subsequently, the snap switch is placed at the top of the platform to control the activation of the LED. The total dimensions of this portable platform were 44.0 mm, 71.0 mm, and 36.0 mm

(width x length x height), as shown in **Fig. 1b**. The platform was fabricated through 3D printing using matte black PLA filament on an Ultimaker S5 fused deposition modelling printer. (Utrecht, Netherlands). Furthermore, we can affirm that this manufacturing process yields a smooth finish with high accuracy, approximately 100.0 μm , along with a rapid fabrication time of 6 hr and 30 min. Leveraging 3D printing and its seamless integration, the proposed μPADs platform offers enhanced portability, affordability, and ease of both manufacturing and utilization.

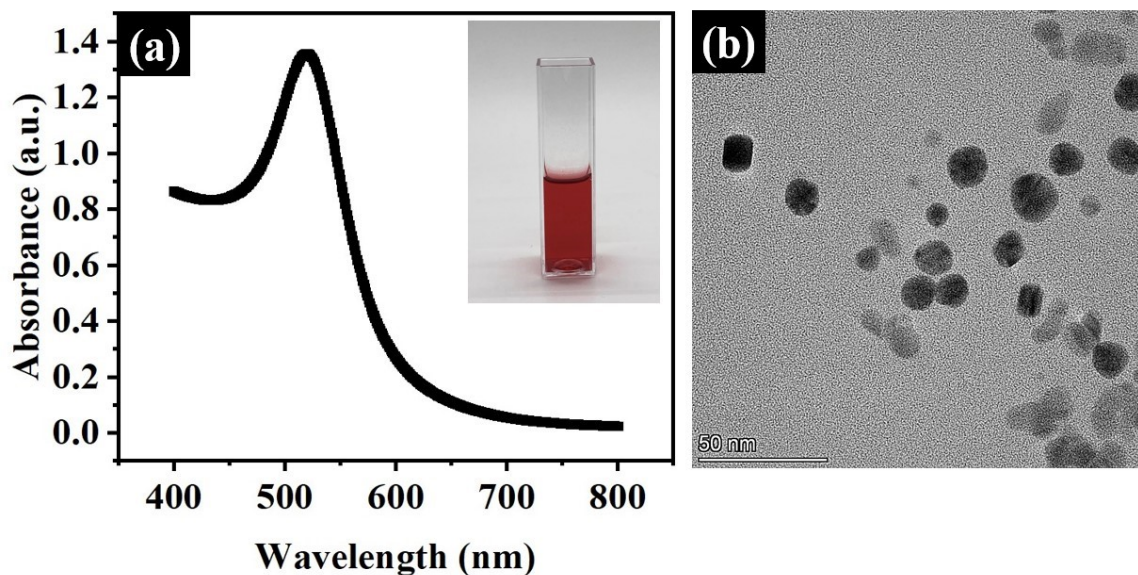


Fig. S1 AuNP characteristics: (a) The absorbance spectrum (its color in inserted image) and (b) TEM image of the AuNPs.

The absorbance spectrum of AuNPs displayed a maximum wavelength at 520.7 nm with the red solution (**Fig. S1(a)**). Their TEM images illustrated the spherical shape with dimensional 10.0 ± 1.0 nm (**Fig. S1(b)**). These above characterizations could confirm the AuNP in this method.

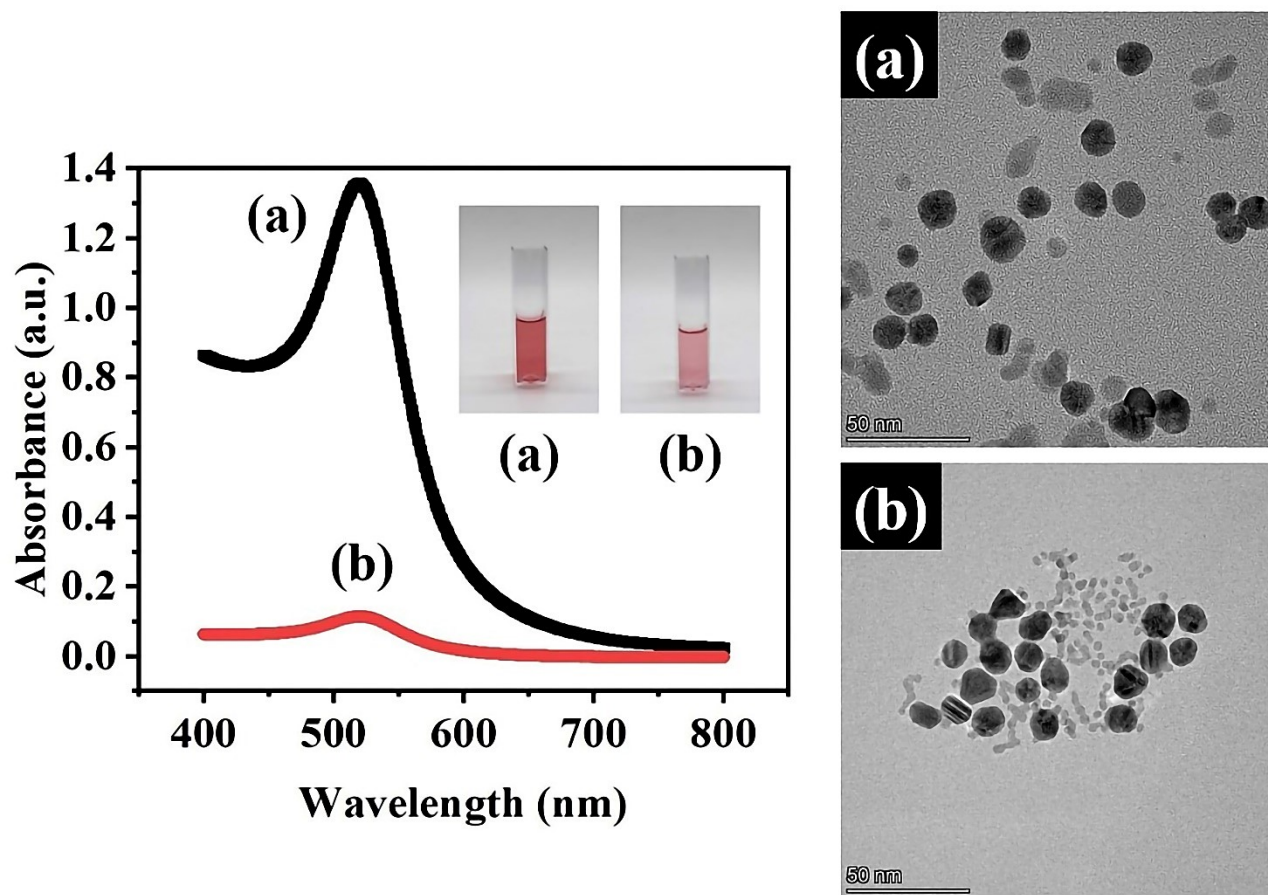


Fig. S2 The absorbance spectrum and TEM image of AuNPs solution with (a) PBS solution and (b) glucose solution at $10.0 \mu\text{mol L}^{-1}$.

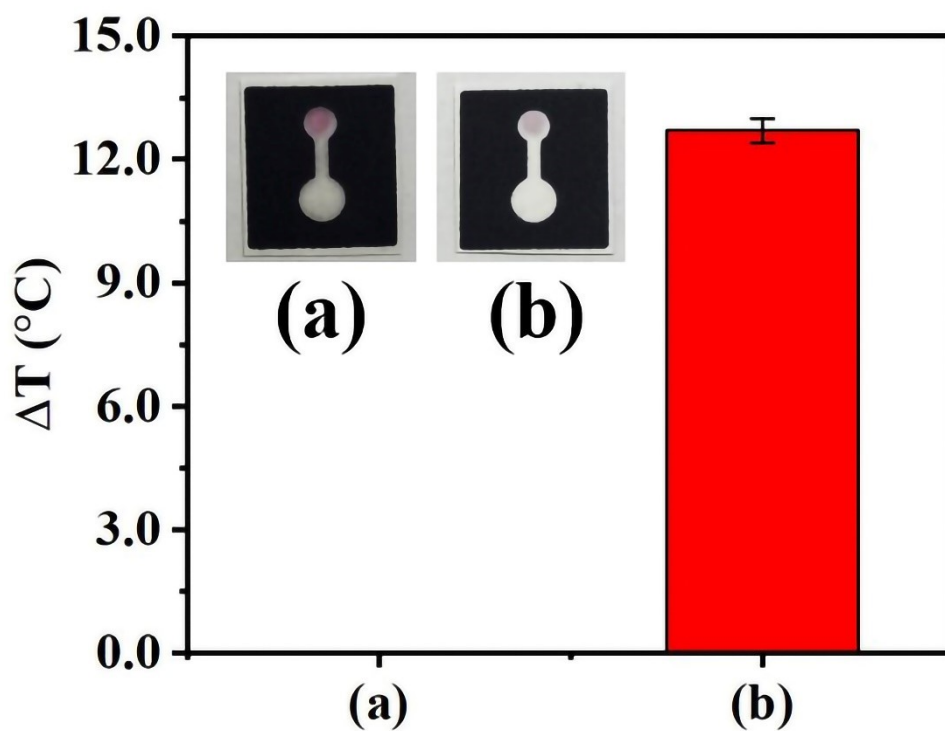


Fig. S3 The displays of μ PADs and the temperature signals of (a) blank and (b) glucose concentration at $10.0 \mu\text{mol L}^{-1}$ using our developed method ($n = 3$).

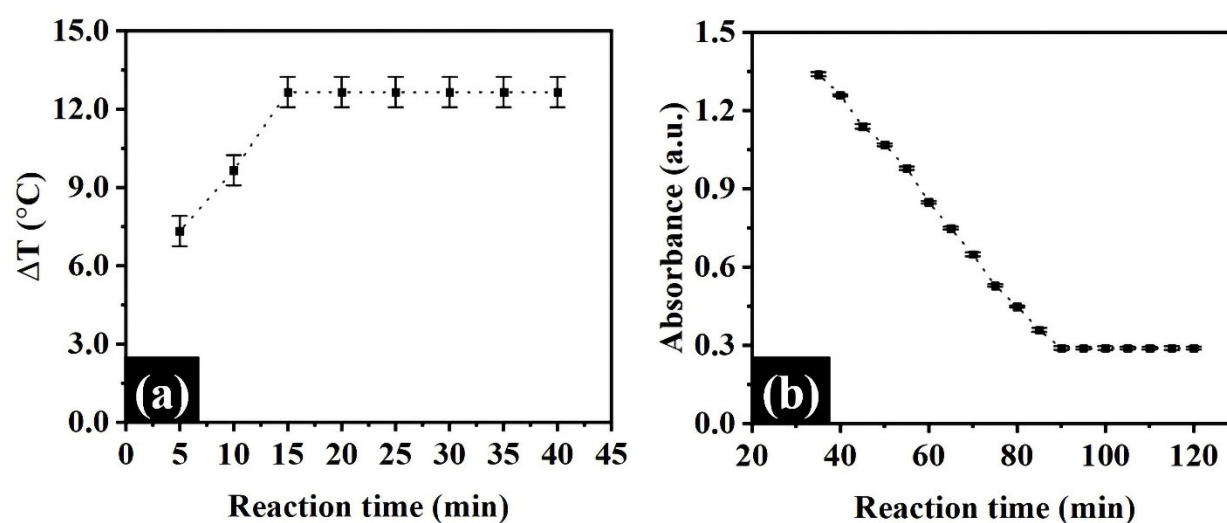


Fig. S4 Demonstrate the reaction time for glucose detection at $10.0 \mu\text{mol L}^{-1}$ using (a) the developed μ PAD sensor and (b) the absorbance detection ($n = 3$).

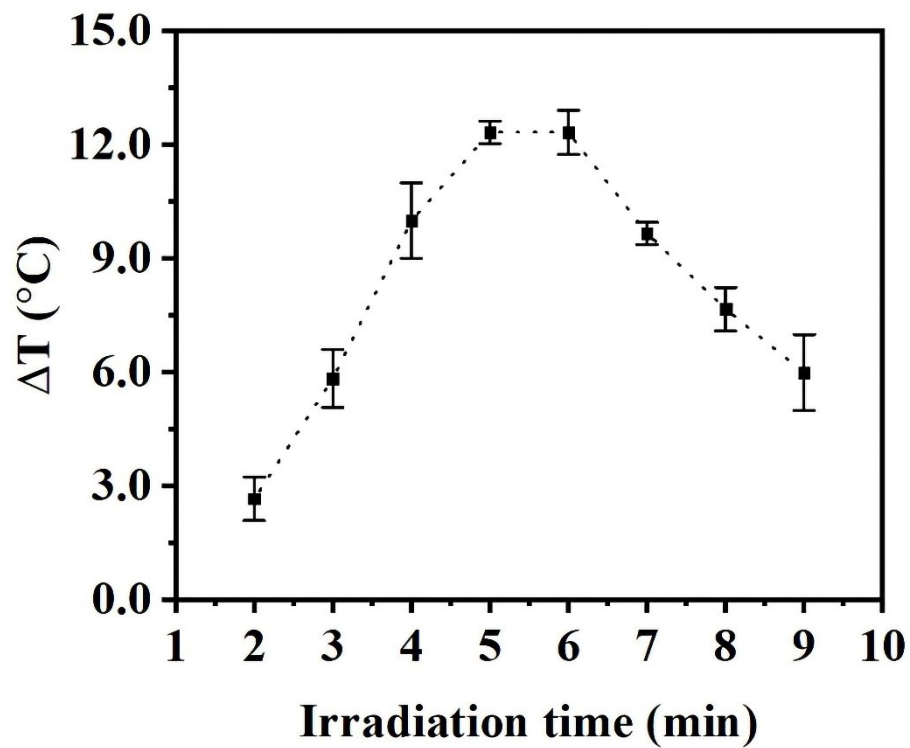


Fig. S5 Demonstrate the temperature signal of irradiation time for glucose detection at $10.0 \mu\text{mol L}^{-1}$ ($n = 3$).

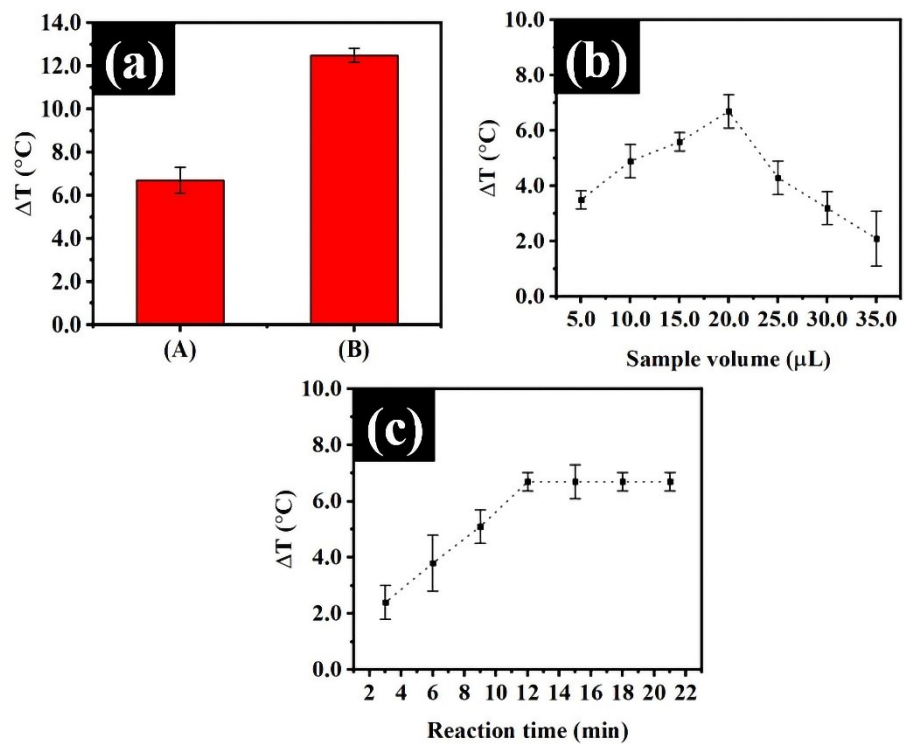


Fig. 6 Demonstrate the temperature signal for (a) comparison between (A) paper spot and (B) the proposed μPAD format for glucose detection at $10.0 \mu\text{mol L}^{-1}$, and (b) sample volume and (c) reaction time for glucose detection at $10.0 \mu\text{mol L}^{-1}$ using paper spot format ($n = 3$).

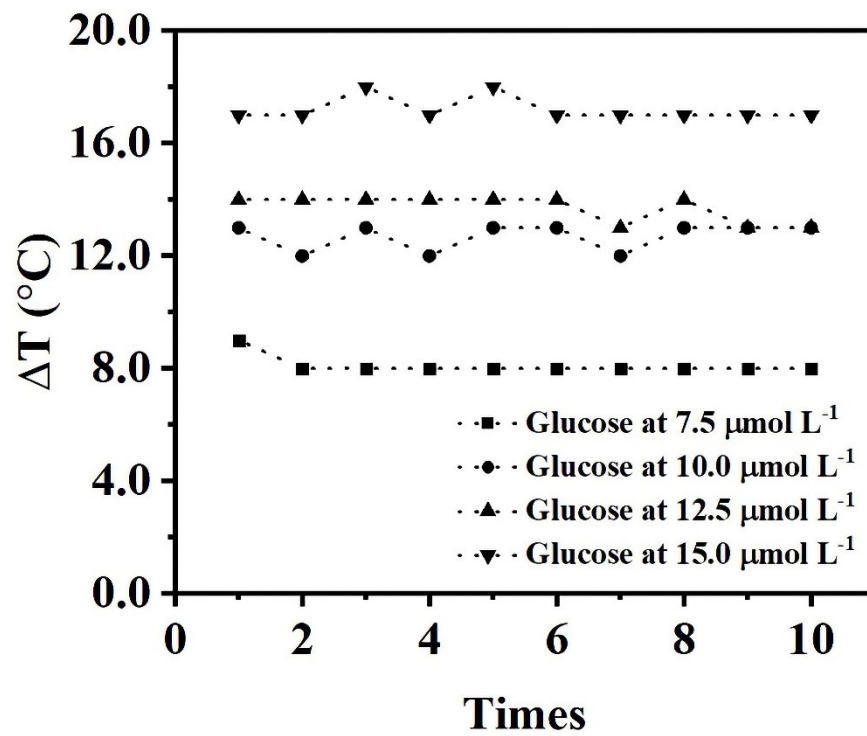


Fig. S7 Demonstrate the temperature signals of reproducibility for glucose detection at different concentration at (■) 7.5 , (●) 10.0 , (▲) 12.5 , and (▼) $15.0 \mu\text{mol L}^{-1}$.

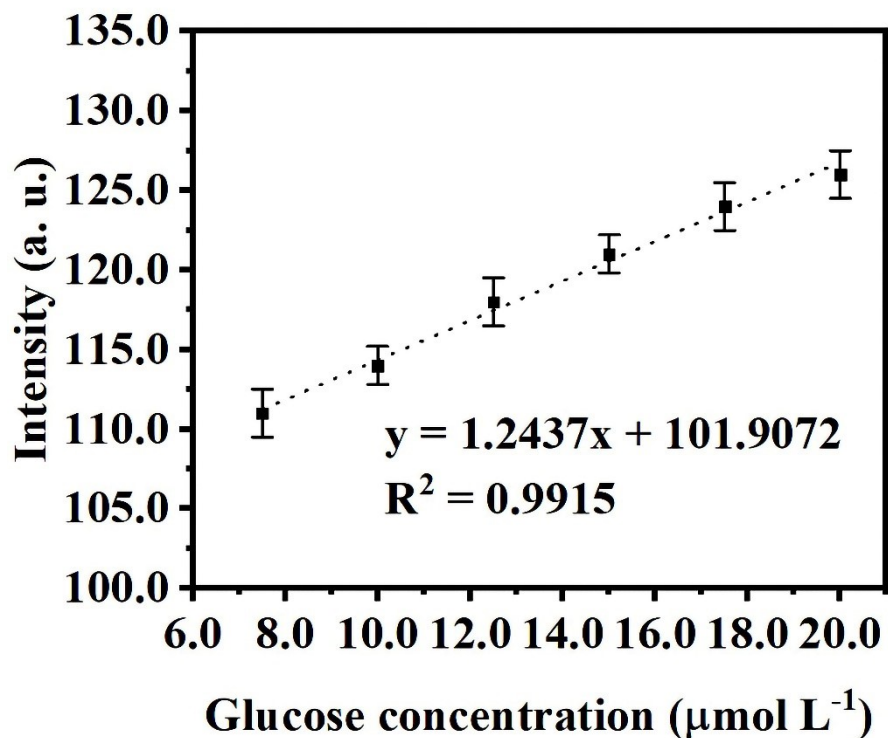


Fig. S8 The linear range of the glucose quantification by colorimetric detection in the proposed method ($n = 3$).

In this experiment, we introduced 30.0 μL of standard glucose at different concentrations into the developed μPADs and allowed them to dry at room temperature for 15 min. Afterwards, the device was inserted into the 3D-box channel to control the light and focusing distance between the device and the smartphone's camera. Subsequently, pictures were taken using the smartphone's camera (iPhone 11), and the color intensity was determined using the Image J software program.

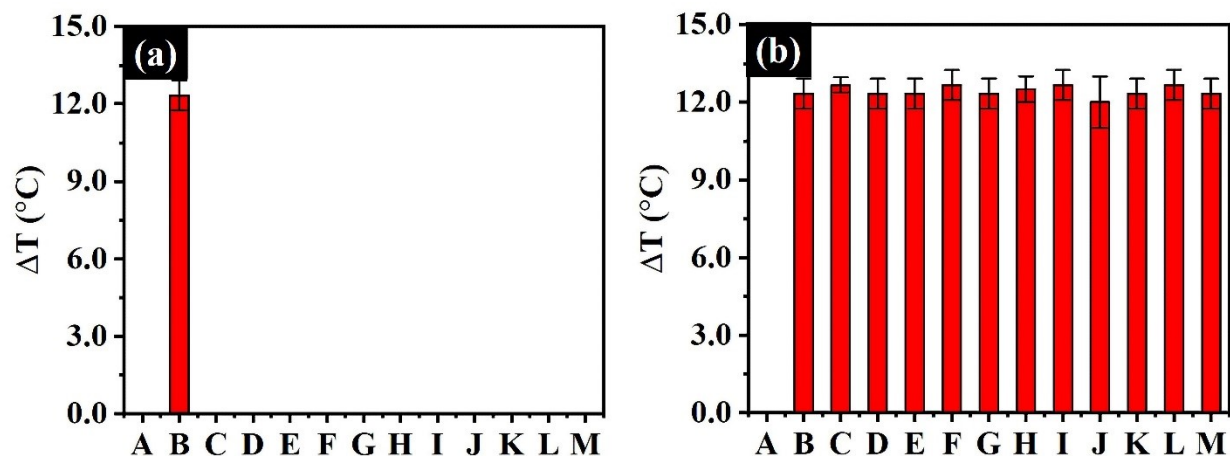


Fig. S9 Demonstrate the selectivity and interference for glucose detection; (a) temperature signals obtained for (A) a blank solution, (B) glucose ($10.0 \mu\text{mol L}^{-1}$), and solutions of a range of potentially interfering substances including (C) BSA ($100.0 \text{ mmol L}^{-1}$), (D) CRP (12.0 mmol L^{-1}), (E) creatinine (1.0 mmol L^{-1}), (F) cortisol (50.0 mmol L^{-1}), (G) dopamine (50.0 nmol L^{-1}), (H) fructose (10.0 mmol L^{-1}), (I) IL-6 ($120.0 \text{ nmol L}^{-1}$), (J) lactic acid ($50.0 \mu\text{mol L}^{-1}$), (K) TNF- α (10.0 pmol L^{-1}), (L) urea (50.0 mmol L^{-1}), and (M) uric acid ($50.0 \mu\text{mol L}^{-1}$). In (b) temperature signal measured for (A) a blank, (B) glucose ($10.0 \mu\text{mol L}^{-1}$), and (C-M) mixtures of glucose ($10.0 \mu\text{mol L}^{-1}$) and above concentrations of the potentially interfering substances ($n = 3$).

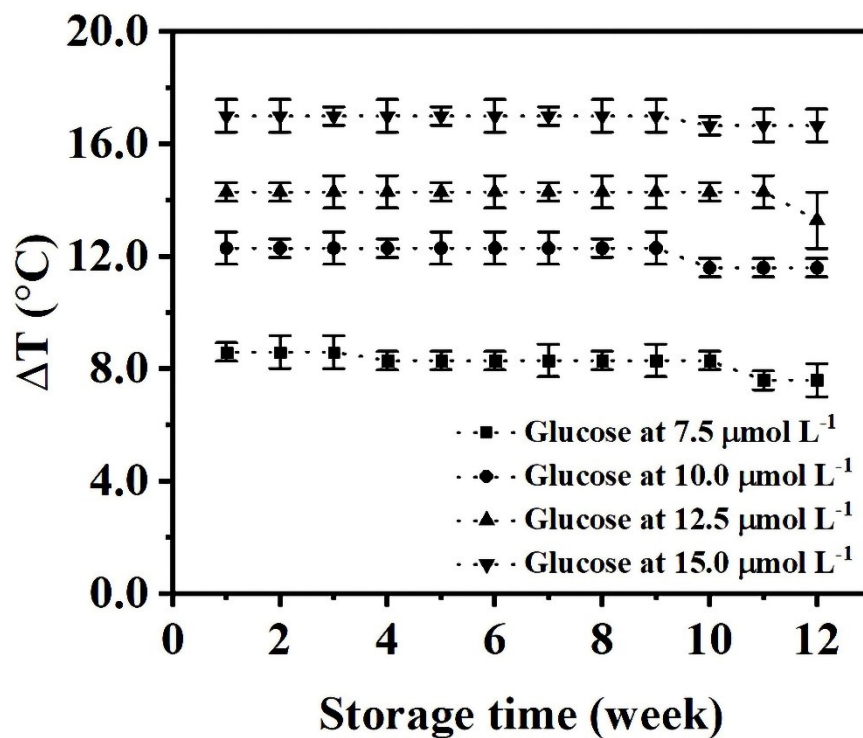


Fig. S10 Demonstrate the temperature signals of storage time of the developed μPADs sensor for glucose detection at different concentration at (\blacksquare) 7.5, (\bullet) 10.0, (\blacktriangle) 12.5, and (\blacktriangledown) 15.0 $\mu\text{mol L}^{-1}$ ($n = 3$).

Table S1 Result of the recovery studies for glucose detection in human control serum samples using our proposed method (n = 3).

Glucose standard added (mmol L⁻¹)	Total found ± S.D. (mmol L⁻¹)	Glucose meter (mmol L⁻¹)	%Recovery	%RSD
0.0	5.29 ± 0.14	5.3	99.73	3.33
2.5	7.83 ± 0.29	7.9	100.38	3.15
5.0	10.31 ± 0.29	10.3	101.03	2.28
7.5	12.82 ± 0.29	12.8	100.97	1.88
10.0	15.35 ± 0.38	15.3	100.91	2.13

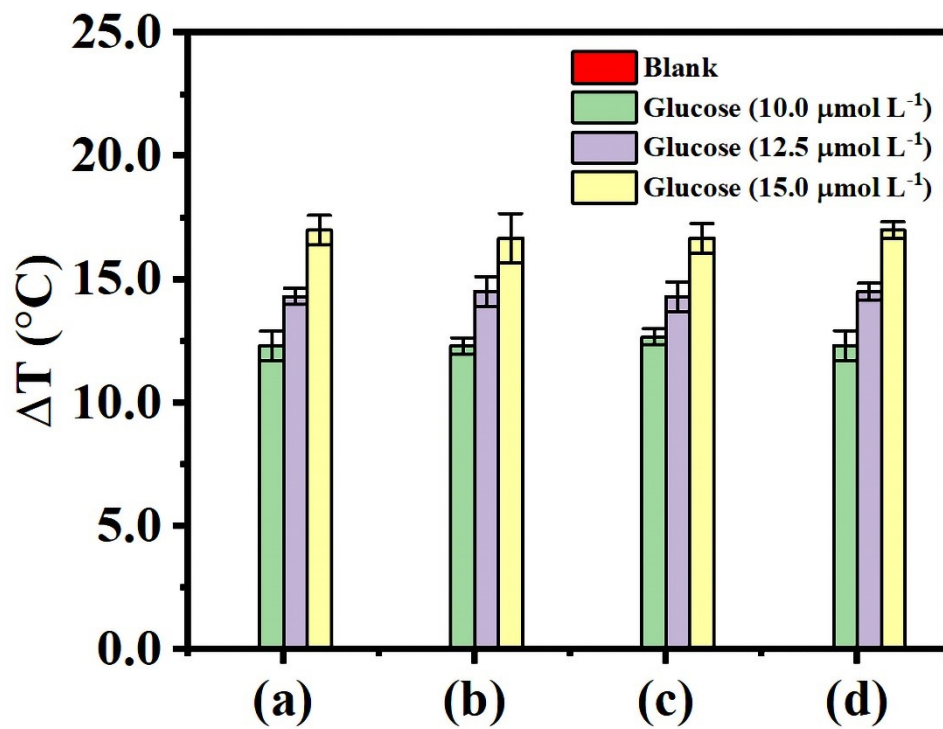


Fig. S11 Demonstrate the ΔT signals of glucose detection in the various sample matrices including (a) PBS, (b) human control serum, (c) human control urine, and (d) artificial saliva ($n = 3$).